

A STEP - UP DC - DC RESONANT CONVERTER FOR GRID - CONNECTED PV SOURCES

GOKULAKRISHNAN , DR.V.GEETHA

Abstract— With the rapid development of large scale renewable energy sources and HVDC grid, it is a promising option to connect the renewable energy sources to the HVDC grid with pure DC system, in which high – power , high - voltage , step - up DC-DC converters are the key equipment to transmit the electrical energy. A resonant converter which is suitable for grid - connected renewable energy sources. The converter can achieve high voltage-gain using LC parallel resonant tank. It is characterized by zero voltage switching (ZVS) turn - on and nearly ZVS turn-off of main switches as well as zero - current - switching (ZCS) turn-off of rectifier diodes, moreover, the equivalent voltage stress of the semiconductor devices is lower than other resonant step - up converters. The operation principle of the converter and its resonant parameter selection is presented in the paper. The operation principle of the proposed converter has been successfully verified by simulation and experiment results.

Keywords -- Resonant converter, voltage step-up, renewable energy, soft switching, voltage stress

I. INTRODUCTION

The development of renewable energy sources is crucial to relieve the pressures of exhaustion of the fossil fuel and environmental pollution. At present, most of the renewable energy sources are utilized with the form of AC power. The generation equipments of the renewable energy sources and energy storage devices usually contain DC conversion stages and the produced electrical energy is delivered to the power grid through DC/AC stages, resulting in additional energy loss. Moreover, the common problem of the renewable energy sources, such as wind and solar, is the large variations of output power, and the connection of large scale of the renewable sources to the power grid is a huge challenge for the traditional electrical equipment, grid structure and operation. DC grid, as one of the solutions to the aforementioned issues, is an emerging and promising approach which has been drawn much attention recently.

At present, the voltages over the DC stages in the generation equipments of the renewable energy sources are relatively low, in the range of several hundred volts to several thousand volts, hence, high-power high-voltage step-up DC-

DC converters are required to deliver the produced electrical energy to HVDC grid. Furthermore, as the connectors between the renewable energy sources and HVDC grid, the step- up DC-DC converters not only transmit electrical energy, but also isolate or buff kinds of fault conditions, they are one of the key equipments in the DC grid.

Recently, the high-power high-voltage step-up DC-DC converters have been studied extensively. The transformer is a convenient approach to realize voltage step-up. The classic full-bridge (FB) converter, single active bridge (SAB) converter and LCC resonant converter are studied and their performance is compared for the offshore wind farm application. The three-phase topologies, such as three-phase SAB converter, series resonant converter and dual active bridge (DAB) converter, which are more suitable for high-power applications due to alleviated current stress of each bridge, are also studied and designed for high-power high-voltage step-up applications. The emerging modular DC-DC converter, which uses two modular multilevel converters (MMC) linked by a medium-frequency transformer, is well suited for the application in the HVDC grid. For these isolated topologies, the main obstacle is the fabrication of the high-power high-voltage medium-frequency transformer and there is no report about the transformer prototype yet. Multiple small-capacity isolated converters connected in series and/or parallel to form a high-power high-voltage converter is an effective means to avoid the use of single large-capacity transformer .

For the application where galvanic isolation is not mandatory, the use of a transformer would only increase the cost, volume and losses, especially for high-power high-voltage applications. Several non-isolated topologies for high-power high-voltage applications have recently been proposed and studied in the literature. A Boost converter is adapted by the researchers of Convertteam company to transmit energy from $\pm 50\text{kV}$ to $\pm 200\text{kV}$. To obtain the higher voltage-gain, Enjeti *et al* proposed a multiple-module structure, which consists of a Boost converter and a Buck/Boost converter connected in input- parallel output-series. The output power and voltage are shared by the two converters and the voltage and current ratings of switches and diodes are correspondingly reduced. However, the efficiency of Boost or Buck/Boost converter is relatively low due to the hard switching of the active switch and the large reverse recovery loss of the diode.

The soft-switching technology is critical to improve the conversion efficiency, especially for high-voltage applications. Recently, several soft-switching topologies for high-power

high-voltage applications have been proposed. In the converter topologies based on resonant switched-capacitor (RSC) are proposed with reduced switching loss and modular structure. The shortage of the RSC based converter is the poor voltage regulation and the requirement of a large number of capacitors. Jovicic *et al* proposed a novel type of resonant step-up converter with potentially soft-switching operation, which utilizes thyristors as switches and does not suffer from excessive switch stresses and reverse recovery problems, moreover, a large voltage-gain is easily to be obtained. Similarly, in a new family of resonant transformerless modular DC-DC converters is proposed and the main feature of the proposed converters is that the unequal voltage stress on semiconductors of thyristor valve is avoided with the use of active switching network, which is composed of an ac capacitor and four identical active switches. Thyristors have large voltage and current ratings; however, the use of thyristor limits the switching frequency of the converter, resulting in bulky passive components and slow dynamic response. Moreover, the resonant inductors of the converters are unidirectional magnetized in, leading to lower utilization of the magnetic core, which means that a great volume of core is required.

In this paper, a novel resonant step-up DC-DC converter is proposed, which not only can realize soft-switching for main switches and diodes and large voltage-gain, but also has relatively lower equivalent voltage stress of the semiconductor devices and bidirectional magnetized resonant inductor. The operation principle of the converter and the design of the resonant parameters are presented in the paper. A 100V(±20%)/1000V, 1kW prototype is built in the lab to verify the effectiveness of the converter.

II. CONVERTER STRUCTURE AND OPERATION PRINCIPLE

The proposed resonant step-up converter is shown in Fig. 1. The converter is composed of a full-bridge switch network, which is made up by Q_1 through Q_4 , a LC parallel resonant tank, a voltage doubler rectifier and two input blocking diodes, D_{b1} and D_{b2} . The steady-state operating waveforms are shown in Fig. 2 and detailed operation modes of the proposed converter are shown in Fig. 3. For the proposed converter, Q_2 and Q_3 are tuned on and off simultaneously, Q_1 and Q_4 are tuned on and off simultaneously. In order to simplify the analysis of the converter, the following assumptions are made:

- 1) all switches, diodes, inductor and capacitor are ideal components;
- 2) output filter capacitors C_1 and C_2 are equal and large enough so that the output voltage V_o is considered constant in a switching period T_s .

Mode 1 [t_0, t_1] [Fig. 3(a)]

During this mode, Q_1 and Q_4 are turned on resulting in the positive input voltage V_{in} across the LC parallel resonant tank, i.e., $v_{Lr}=v_{Cr}=V_{in}$. The converter operates similar to a

conventional Boost converter and the resonant inductor L_r acts as the Boost inductor with the

current through it increasing linearly from I_0 . The load is powered by C_1 and C_2 . At t_1 , the resonant inductor current i_{Lr} reaches I_1 .

$$I_1 = I_0 + \frac{V T}{L_r} \quad (1)$$

where T_1 is the time interval of t_0 to t_1 .

In this mode the energy delivered from V_{in} to L_r is

$$E_{in} = \frac{1}{2} L_r (I_1^2 - I_0^2) \quad (2)$$

Mode 2 [t_1, t_3] [Fig. 3(b)]

At t_1 , Q_1 and Q_4 are turned off and after that L_r resonates with C_r , v_{Cr} decreases from V_{in} and i_{Lr} increases from I_1 in resonant form. Taking into account the parasitic output

capacitors of Q_1 through Q_4 and junction capacitor of D_{b2} , the equivalent circuit of the converter after t_1 is shown in Fig. 4(a), in which C_{Db2} , C_{Q1} and C_{Q4} are charged, C_{Q2} and C_{Q3} are discharged. In order to realize zero-voltage-switching (ZVS) for Q_2 and Q_3 , an additional capacitor, whose magnitude is about 10 times

with respect to C_{Q2} , is connected in parallel with D_{b2} . Hence, the voltage across D_{b2} is considered unchanged during the charging/discharging process and D_{b2} is equivalent to be shorted. Due to C_r is much larger than the parasitic capacitances, the voltages across Q_1 and Q_4 increase slowly. As a result, Q_1 and Q_4 are turned off at almost zero voltage in this mode.

When v_{Cr} drops to zero, i_{Lr} reaches its maximum magnitude. After that, v_{Cr} increases in negative direction and i_{Lr} declines in resonant form. At t_2 , $v_{Cr} = -V_{in}$, the voltages across Q_1 and Q_4 reach V_{in} , the voltages across Q_2 and Q_3 fall to zero and the two switches can be turned on under zero-voltage condition. It should be noted that although Q_2 and Q_3 could be turned on after t_2 , there are no currents flowing through them. After t_2 , L_r continues to resonate with C_r , v_{Cr} increases in negative direction from $-V_{in}$, i_{Lr} declines in resonant form. D_{b2} will hold reversed-bias voltage and the voltage across Q_4 continues to increase from V_{in} . The voltage across Q_1 is kept at V_{in} . The equivalent circuit of the converter after t_2 is shown in Fig. 4(b), in which D_2 and D_3 are the anti-parallel diodes of Q_2 and Q_3 , respectively. This mode runs until v_{Cr} increases to $-V_o/2$ and i_{Lr} reduces to I_2 , at t_3 , the voltage across Q_4 reaches $V_o/2$ and the voltage across D_{b2} reaches

$$V_o/2 - V_{in}.$$

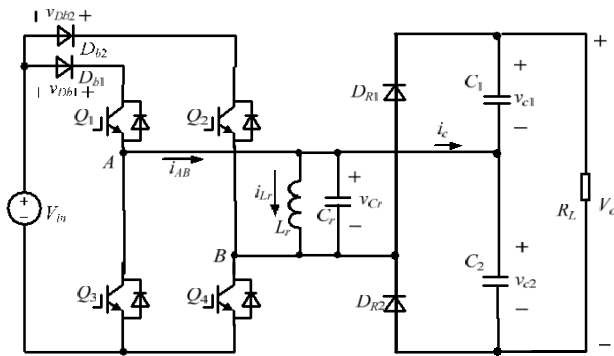


Figure 1. Topology of proposed resonant step-up converter.

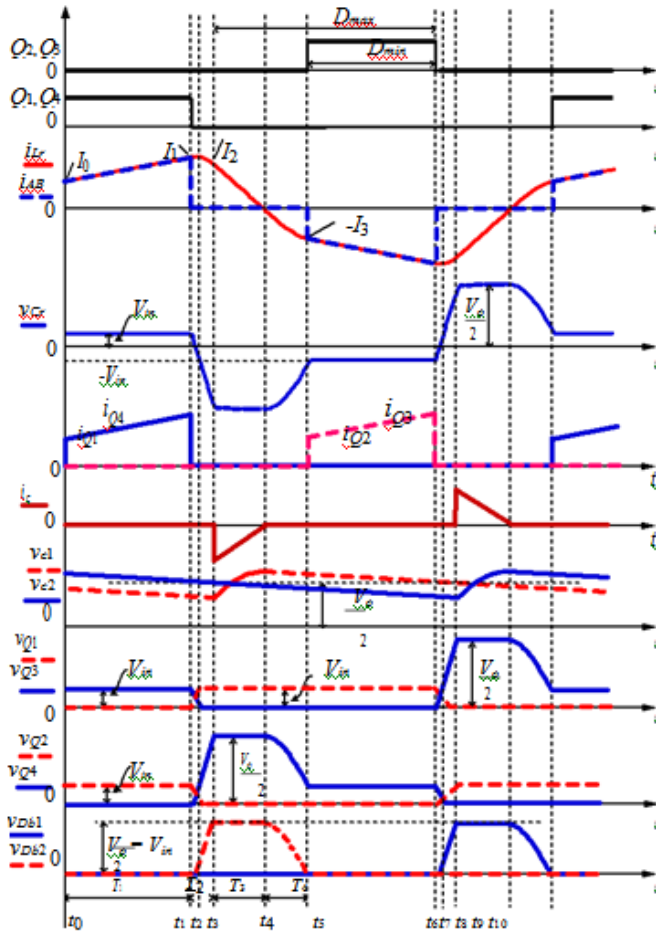
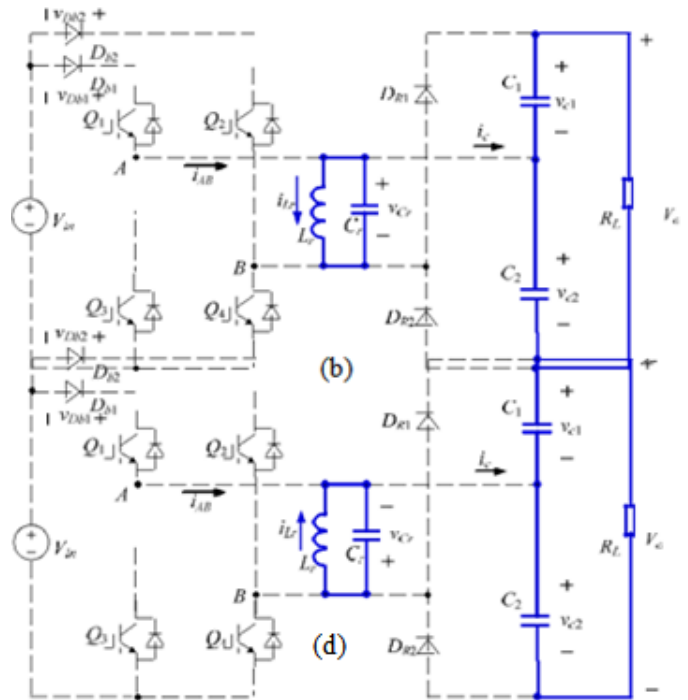
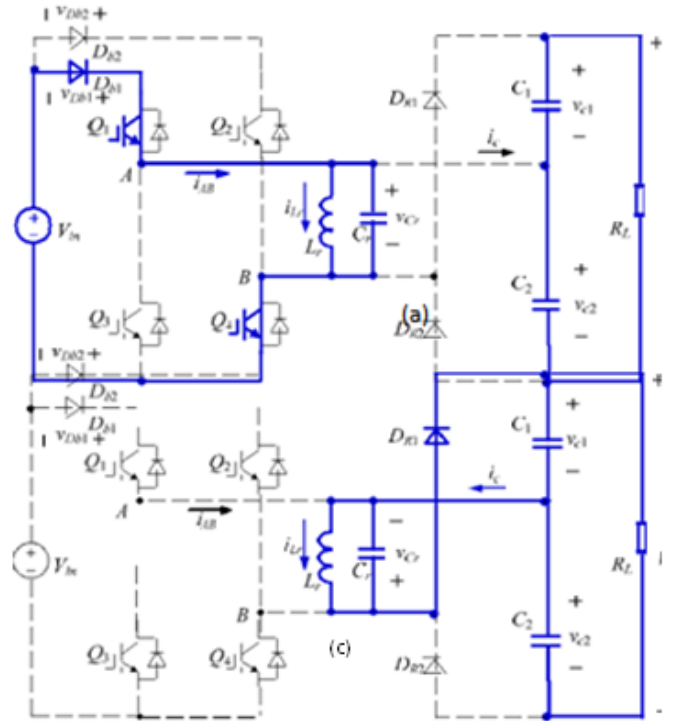


Figure 2. Operating waveforms of the proposed converter.



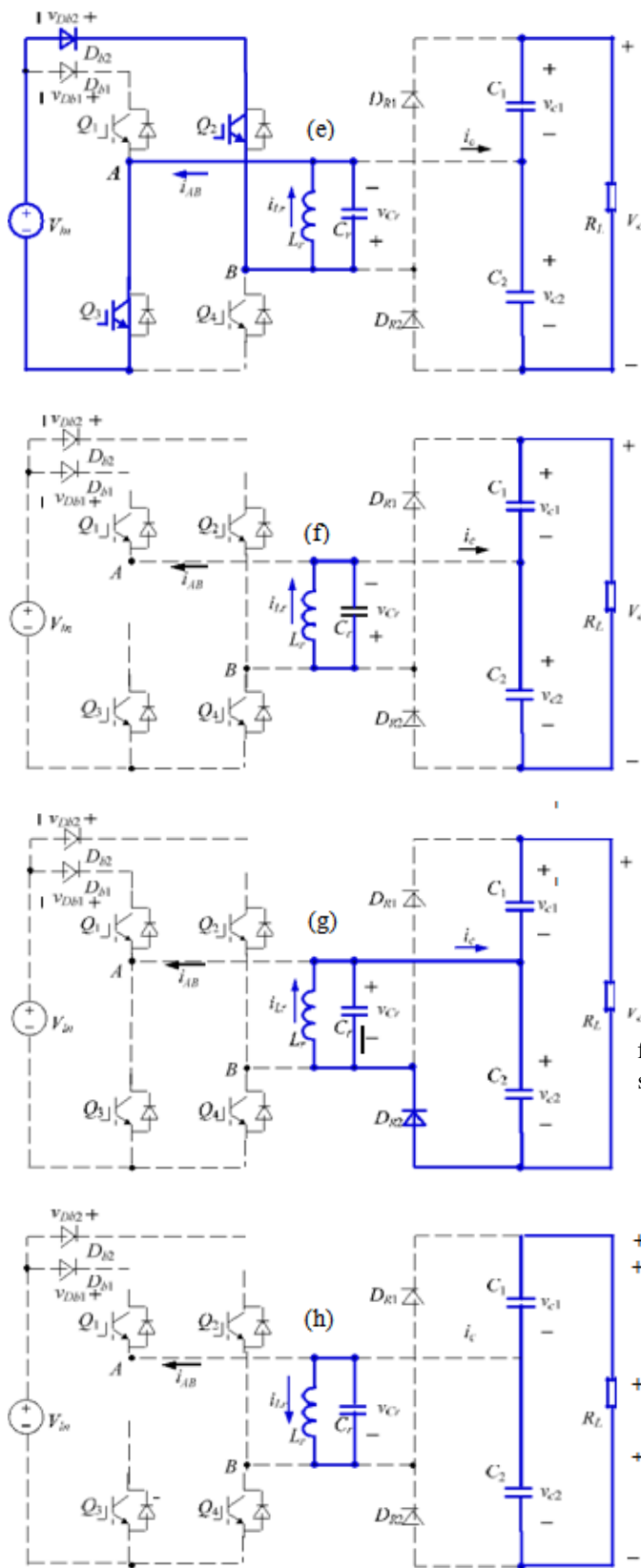


Figure 3. Equivalent circuits of each operation stages. (a) [t0, t1]. (b) [t1, t3]. (c) [t3, t4]. (d) [t4, t5]. (e) [t5, t6]. (f) [t6, t8]. (g) [t8, t9]. (h) [t9, t10].

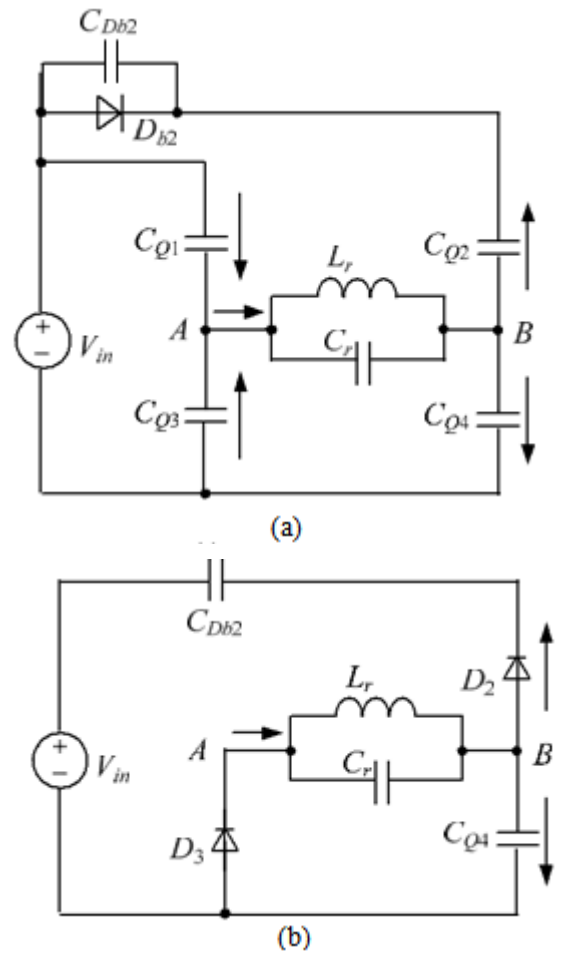


Figure 4. Further equivalent circuits of Mode 2. (a) [t1, t2]. (b) [t2, t3].

It can be seen that during \$t_1\$ to \$t_3\$ no power is transferred from the input source or to the load, and the whole energy stored in LC resonant tank is unchanged, i.e.,

$$\frac{1}{2} L I^2 + \frac{1}{2} C V^2 = \frac{1}{2} L I^2 + \frac{1}{2} C (V_o)^2 \quad (3)$$

We have

$$i(t) = \frac{V}{Z_r} \sin[\omega(t-t_1)] + I \cos[\omega(t-t_1)] \quad (4)$$

$$v(t) = V \cos[\omega(t-t_1)] - I Z_r \sin[\omega(t-t_1)] \quad (5)$$

$$T_2 = \frac{1}{\omega_r} \arcsin \frac{V}{\sqrt{V^2 + \frac{LI^2}{C_r}}} + \arcsin \frac{V_o}{\sqrt{V^2 + \frac{LI^2}{C_r}}} \quad (6)$$

where $\omega_r = 1/\sqrt{L_r C_r}$, $Z_r = L_r \omega_r / T_2$ is the time interval of \$t_1\$ to \$t_3\$.

At t_3 , $v_{Cr} = -V_o/2$, $DR1$ conducts naturally, $C1$ is charged by i_{Lr} through $DR1$, v_{Cr} keeps unchanged, i_{Lr} decreases linearly. At t_4 , $i_{Lr} = 0$. The interval of T_3 , T_4 .

$$T_3 = \frac{2I_{2r}L}{V_o} \quad (7)$$

The energy delivered to load side in this mode is

$$E_{out} = \frac{V_o I_{2r} T_3}{4} \quad (8)$$

The energy consumed by the load in half switching period is

$$E_R = \frac{V_o I_o T_1}{2} \quad (9)$$

Assuming 100% conversion efficiency of the converter and according to the energy conversation rule, in half switching period,

$$E_{in} = E_{out} = E_R \quad (10)$$

Combining (7), (8), (9) and (10), we have

$$I_{2r} = V_o \sqrt{\frac{I_o T_1}{V L}} \quad (11)$$

$$T_3 = 2 \sqrt{\frac{I_o T_1 L}{V_o}} \quad (12)$$

(4) Mode 4 [t_4 , t_5] [Fig. 3(d)]

At t_4 , i_{Lr} decreases to zero and the current flowing through $DR1$ also decreases to zero, and $DR1$ is turned off with zero-current- switching (ZCS), therefore, there is no reverse recovery. After t_4 , L_r resonates with C_r , C_r is discharged through L_r , v_{Cr} increases from $-V_o/2$ in positive direction, i_{Lr} increases from zero in negative direction. Meanwhile, the voltage across $Q4$ declines from

$V_o/2$. At t_5 , $v_{Cr} = -V_{in}$, $i_{Lr} = -I_3$. In this mode, the whole energy stored in LC resonant tank is unchanged, i.e.,

$$\frac{1}{2} C (V_o)^2 = \frac{1}{2} L I^2 + \frac{1}{2} C V^2 \quad (13)$$

We have

$$I_0 = I_3 = \frac{1}{2} \sqrt{\frac{C (V_o^2 - 4V_{in}^2)}{L}} \quad (14)$$

$$i_{Lr}(t) = -\frac{V_o}{2\omega_r L_r} \sin[\omega_r(t - t_4)] \quad (15)$$

$$v_{Cr}(t) = \frac{-V_o \cos[\omega_r(t - t_4)]}{2} \quad (16)$$

$$T_4 = \frac{1}{\omega} \arccos\left(\frac{2V_{in}}{V_o}\right) \quad (17)$$

where T_4 is the time interval of t_4 to t_5 . (5) Mode 5 [t_5 , t_6] [Fig. 3(e)]

If Q_2 and Q_3 are turned on before t_5 , then after t_5 , L_r is charged by V_{in} through Q_2 and Q_3 , i_{Lr} increases in negative direction, the mode is similar to Mode 1.

If Q_2 and Q_3 are not turned on before t_5 , then after t_5 , L_r will resonate with C_r , the voltage of node A v_A will increase from zero and the voltage of node B v_B will decay from V_{in} . Zero-voltage condition will be lost if Q_2 and Q_3 are turned on at the moment. Therefore, Q_2 and Q_3 must be turned on before t_5 to reduce switching loss.

TABLE I - COMPARISON OF DIFFERENT NON-ISOLATED CONVERTER TOPOLOGIES

Topologies	Voltage stress	Soft switching	Voltage regulation	Switching frequency	Output fault shorts input	Input fault shorts output
Refs.[22, 23]	Low	No	Good	Constant	Yes	No
Refs.[24, 25]	Low	Yes	Poor	Constant	Yes	Yes
Refs.[26-28]	High	Yes	Good	Variable	No	No
Ref.[29]	High	Yes	Good	Variable	Yes	No
Proposed one	Medium	Yes	Good	Variable	No	No

The operation modes during [t_6 , t_{10}] are similar to the modes 2, 3 and 4, and the detailed equivalent circuits are

shown in Fig. 3 (f), (g) and (h). During [t_6 , t_{10}], Q_2 and Q_3 are turned off at almost zero voltage, Q_1 and Q_4 are turned on with ZVS, and $DR2$ is turned off with ZCS.

III. ANALYSIS AND DESIGN OF THE CONVERTER

A. Voltage Rating and DC Fault Response

According to the analysis of Section II, the voltage stresses of Q_1 and Q_2 are the input voltage V_{in} , the voltage stresses of Q_3 and Q_4 are half of the output voltage, i.e., $V_o/2$, the voltage stresses of D_{b1} and D_{b2} are $V_o/2 - V_{in}$. The total voltage stress of the primary semiconductor devices is $2V_o$, which is half of that in the Refs. [26-29]. It implies that much less semiconductor devices are required in the proposed step-up converter, resulting in low conduction and switching losses and low cost. Moreover, the peak voltages across the resonant inductor and resonant capacitor are $V_o/2$, which is also half of that in the Refs. [26-29]. Lower peak voltage indicates that the insulation is easy to be implemented, leading to the reduction of the size of the resonant tank.

As shown in Fig. 1, the proposed converter can block an output fault and prevent the fault pass through input side, and vice versa. The comparison of different non-isolated converter topologies is listed in Table I.

B. Voltage balance between C1 and C2

The above analysis is based on the assumption that voltages across C1 and C2 are respectively half of output voltage. Provided that $V \neq V_o$, for example

$V > V_o/2 > V_o/3$, $c_1 < c_2$ according to the operation principle of Fig. 2, the peak current of i at t_1 will be smaller than that at t_2 , which means that the average current flowing into C1 will be smaller than the average current flowing into C2. Due to C1 and C2 power the same load, therefore, V_{C1} decreases and V_{C2} increases, and finally they share the same output voltage. Vice versa, i.e. V_{C1} increases and V_{C2} decreases under the presumption that $V_{C1} < V_o/2 < V_{C2}$.

C. Analysis of the Converter

From Fig. 2, we have

$$T_1 + T_2 + T_3 + T_4 = \frac{T}{2} \quad (18)$$

$$V_o I_o T_1 = \frac{V^2 T_1^2}{L_r} + V T_1 \sqrt{\frac{C(V^2 - 4V_o^2)}{L_r}} \quad (19)$$

From (19), we have

$$T_1 = \frac{\sqrt{\frac{C(V^2 - 4V_o^2)}{L_r}} + \sqrt{\frac{C(V^2 - 4V_o^2)}{L_r}}}{2 \frac{V_o}{V}} \quad (20)$$

From (17), the gain of V_o/V_{in} is expressed as

$$\frac{V_o}{V_{in}} = \frac{2}{\cos(\omega_r T_4)} \quad (21)$$

It can be seen that the gain of V_o/V_{in} is impacted by the parameters of the resonant tank (L_r and C_r) and the time interval of t_4 to t_5 , which is a part of switching period,

hence, in other words, the gain is impacted by L_r , C_r and the switching frequency. Several important conclusions are obtained from (21).

- (1) For any given voltage gain (larger than 2) and the resonant tank parameters L_r and C_r , there must be a T_4 to meet (21), which implies that for given L_r and C_r , the voltage gain can be infinite if the switching frequency range is not taken into account.
- (2) For given voltage gain, the larger the ω_r , the shorter the T_4 , an example is shown in Fig. 5, which means that the switching frequency will be higher.
- (3) For given voltage gain and ω_r , although T_4 is constant, but the expressions of T_1 , T_2 and T_3 are related to L_r or C_r , which means that different pairs of L_r and C_r impact the switching frequency of the proposed converter.

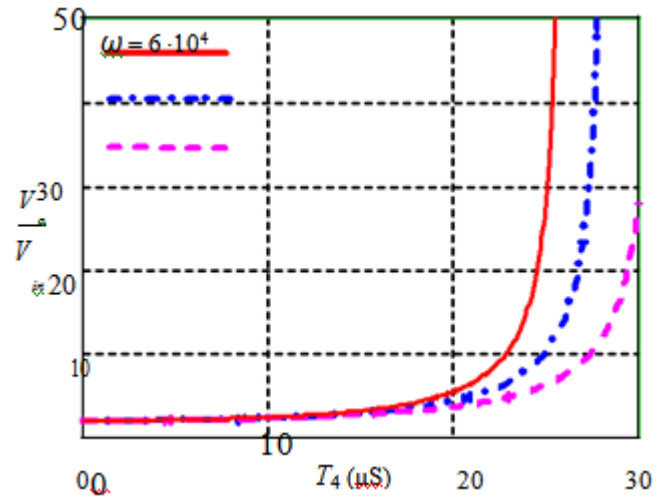


Figure 5. The voltage gain versus ω_r and T_4 .

Substitution (20) into (1), yields,

$$I_1 = \sqrt{\frac{C(V^2 - 4V_o^2) + 4VIT}{4L_r}} \quad (22)$$

Substitution (22) into (3), yields,

$$I_2 = \sqrt{\frac{V_o I_o T_1}{L_r}} \quad (23)$$

Substitution (22) into (6), yields,

$$\frac{1}{\omega_r} = \frac{2V_{in}}{\sqrt{\frac{4V_o I_o T_1}{L_r + C}}} = \frac{V_o}{\sqrt{\frac{4V_o I_o T_1}{L_r + C}}} \quad (24)$$

Combining (12), (17), (18), (20) and (24), we can obtain (25) at the bottom of the page.

From (25) we can obtain the following equation at unloaded condition ($I_o=0$),

$$f_s = f_r \quad (I_o=0) \quad (26)$$

where f_s is the switching frequency and f_r is the resonant frequency of L_r and C_r , i.e.,

$$f_r = \frac{1}{2\pi \sqrt{L_r C_r}} \quad (27)$$

It can be seen that the switching frequency is equal to the resonant frequency at unloaded condition. Actually, it can be seen from Fig. 2 that $T_1=T_3=0$ at unloaded condition because there is no energy input and output if the converter

is assumed to be lossless. And if $I_O > 0$, then both T_1 and T_3 are larger than zero, thus the switching frequency is lower than the resonant frequency, the heavier the load, the lower the switching frequency. Therefore, the maximum switching frequency of the converter is

$$f_{s,max} = f_r \quad (28)$$

From the analysis of Section II, it can be seen that to realize zero-voltage turn-on of the switches, the minimum duty cycle of the converter is

$$D_{min} = \frac{T_1}{T_s} \quad (29)$$

As shown in Fig. 2 and the above analysis, the minimum duty cycle also is the effective duty cycle of the converter, during which the primary current flows through the main switches.

According to (5), the time interval T of t_1 to t_2 is

$$T = \frac{2}{\omega_r} \arccos \left(\frac{2V_{in}}{V_o + \sqrt{\frac{4V_{in}^2}{C_r}}} \right) \quad (30)$$

The maximum duty cycle of the converter is

$$D_{max} = \frac{T_s/2 - T}{T_s} \quad (31)$$

D. Design of the Converter

A five megawatt, 4kV(±10%)/80 kV step-up converter is taken as an example to design the parameters. IGBTs are taken as the main switches and $f_{s,max}$ is set to be 5 kHz.

From (25), one can obtain the expression of T_s associated with L_r at full-load condition. However, Eq. (25) indicates that T_s is an implicit function associated with L_r and the concrete analytic solution of T_s cannot be obtained. With the help of mathematical analysis software Maple, we can obtain the curves between L_r and T under different input voltages as shown in Fig. 6. It can be seen that for given V_o and L_r , the lower the input voltage V_{in} , the lower the switching frequency, and for given input voltage range, the smaller the L_r , the narrower the variation of switching frequency.

From (14), one can obtain the curves between L_r and I_0 under different input voltages, as shown in Fig. 7. Through (22) and (25), one can obtain the curves between L_r and I_1 under different input voltages, as shown in Fig. 7. It can be seen that the input voltage has little influence on I_0 and I_1 , because as shown in (14) and (22), the larger the voltage gain, the less the influence of the input voltage on I_0 and I_1 .

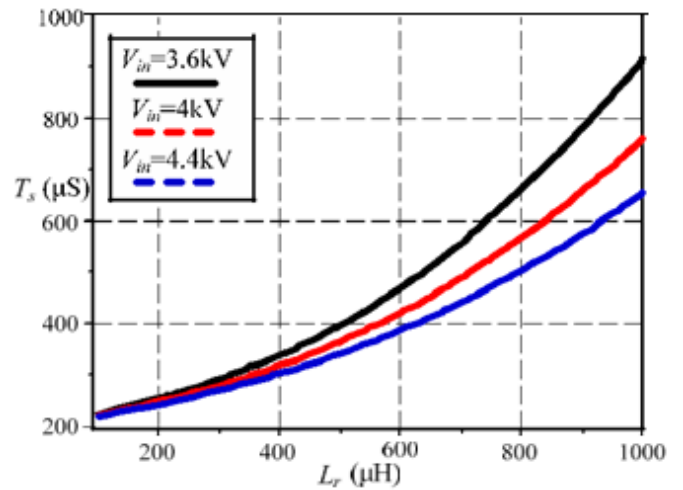


Figure 6. The curves between L_r and T_s under different input voltages.

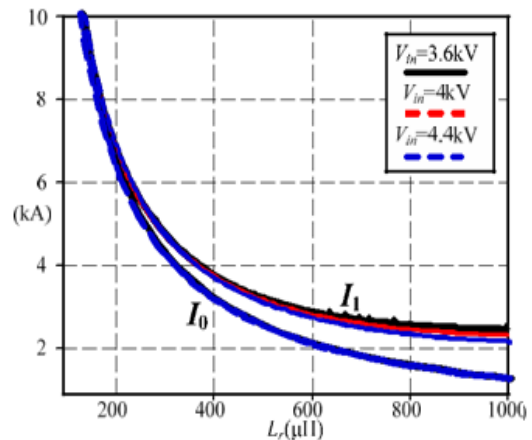


Figure 7. The curves between L_r and I_0, I_1 under different input voltages

From Fig. 6, it can be seen that the smaller the L_r , the shorter the T_s at full-load condition, which means that the converter has relatively narrower range of switching

$$\frac{V_o}{\sqrt{\frac{4V_{in}^2}{C_r} + 2}} = \frac{1}{\sqrt{\frac{I_0 I_1}{V} + \omega \arccos\left(\frac{2V_{in}}{V}\right)}} = 2 \quad (25)$$

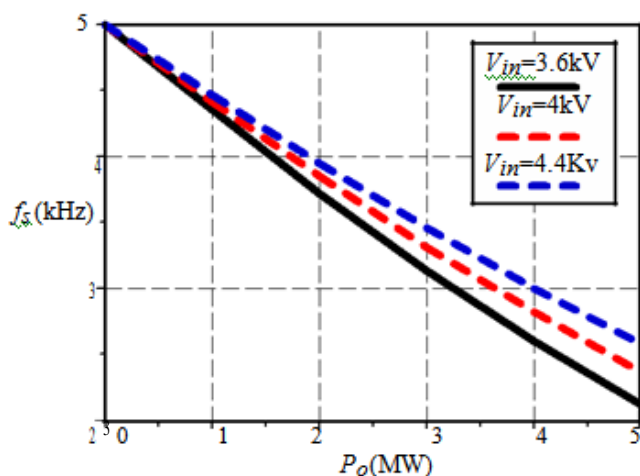


Figure 8. The curves of switching frequency versus output power under different input voltages.

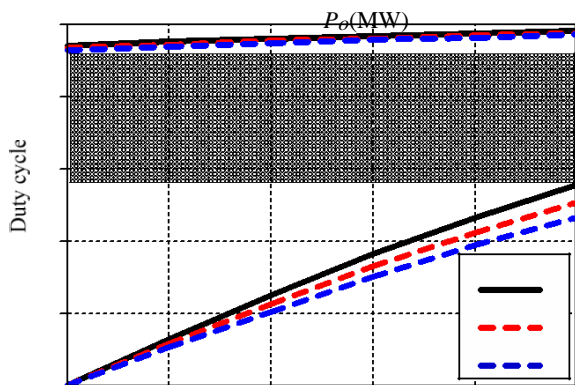


Figure 9. The curves of D_{min} and D_{max} versus output power under different input voltages.

frequency because the maximum switching frequency is fixed, and it is beneficial to the design of input/output filters and resonant inductor. On the contrary, the larger the L_r , the longer the T_S at full-load condition, which means that the converter has relatively wider range of switching frequency and it is disadvantageous to the design of input/output filters and resonant inductor. From Fig. 7 it can be seen that the smaller the L_r , the larger the I_0 and I_1 , which means that switches and diodes have large peak currents and it is harmful for the device choice, while larger L_r is helpful for the device choice. Hence, there is a tradeoff when design the resonant parameters.

The final selection of L_r is 600 μ H, C_r is 1.68 μ F, and the minimum switching frequency is 2.1 kHz, and the peak current of the semiconductor devices is 2850A, which is about two times of the average input current.

After the choice of the resonant parameters, the relationship between the switching frequency and power load is depicted in Fig. 8 with (25). As the figure shows, the range of the switching frequency is 2.1 kHz ~ 5 kHz in the whole load and input voltage range. The switching frequency depends on the output power and the switching frequency drops almost linearly with the increasing of the output power. According to

(29) and (31), the curves of D_{min} and D_{max} with respect to output power under different input voltages are shown in Fig. 9. As the figure shows, both D_{min} and D_{max} depend on the output power, the maximum of D_{min} is 0.277 and the minimum of D_{max} is 0.465. Thus, to realized ZVS for the switches, the duty cycle can be the any value in the range of 0.277 ~ 0.465, as the shaded area shown in Fig. 9. Therefore, the control of the proposed converter is very simple with constant duty cycle and variable switching frequency.

IV. SIMULATION AND EXPERIMENTAL RESULTS

In order to verify the operation principle and the theoretical analysis, a converter is simulated with PLECS simulation software and the detailed parameters are listed in Table II. All switches using in PLECS simulation are ideal switches and 5 nF capacitance is added in parallel with D_{b1} and D_{b2} .

TABLE II SIMULATION PARAMETERS

Item	Symbol	Value
Input voltage	V_{in}	3.6 kV ~ 4.4 kV
Output voltage	V_o	80 kV
Resonant inductance	L_r	600 μ H
Resonant capacitance	C_r	1.68 μ F
Filter capacitance	C_1, C_2	22 μ F
Duty cycle	D	0.4

Fig. 10 shows the simulation results at the output power of 5 MW and 1 MW ($V_{in}=4$ kV), respectively. As the figure shows, the voltage stress of Q_1 and Q_2 is 4 kV, the voltage stresses of Q_3 and Q_4 is 40 kV, the voltage stress of D_{b1} and D_{b2} is 36 kV, the peak voltage across the LC resonant tank is 40 kV, Q_1 through Q_4 are turned on under zero voltage condition and when they are turned off, the voltage across the device increases slowly from zero. The switching frequencies of the converter at 5 MW and 1 MW are 2.3 kHz and 4.4 kHz, respectively. The simulation results match well with the aforementioned analysis.

Fig. 11(a) illustrates the simulation results corresponding to a step change of input voltage from 4 kV to 4.4 kV at full load condition. It can be seen that the output voltage is regulated to be constant and the switching frequency f_s changes from 2.3 kHz to 2.5 kHz. Fig. 11(b) illustrates the simulation results corresponding to a load stepping from full load to 40% load at 4 kV input voltage condition. It can be seen that the output voltage is regulated to be constant and the switching frequency f_s changes from 2.3 kHz to 3.8 kHz.

The simulation results match well with Fig. 8 and the control strategy of variable frequency with constant duty cycle is validated.

The efficiency and losses distribution of the 5 MW condition is also calculated. HiPak IGBT module 5SNA 0600G650100 (6500V, 600A) from ABB is used as the active switches. In the calculation, ten 6500V IGBTs are connected in series to hold up 40 kV. HiPak diode module 5SLD 0600J650100 (6500V, 1200A) from ABB

is used as the input blocking diodes and rectifier diodes. The core material of the resonant inductor is VITROPERM 500F. Suitable high-voltage capacitors are chosen from EACO. The calculated efficiency is around 97.2% and the losses distribution is depicted in Fig. 12.

Figure 10. Steady state simulation results at different load conditions when $V_{in}=4$ kV. (a) 5 MW. (b) 1MW.

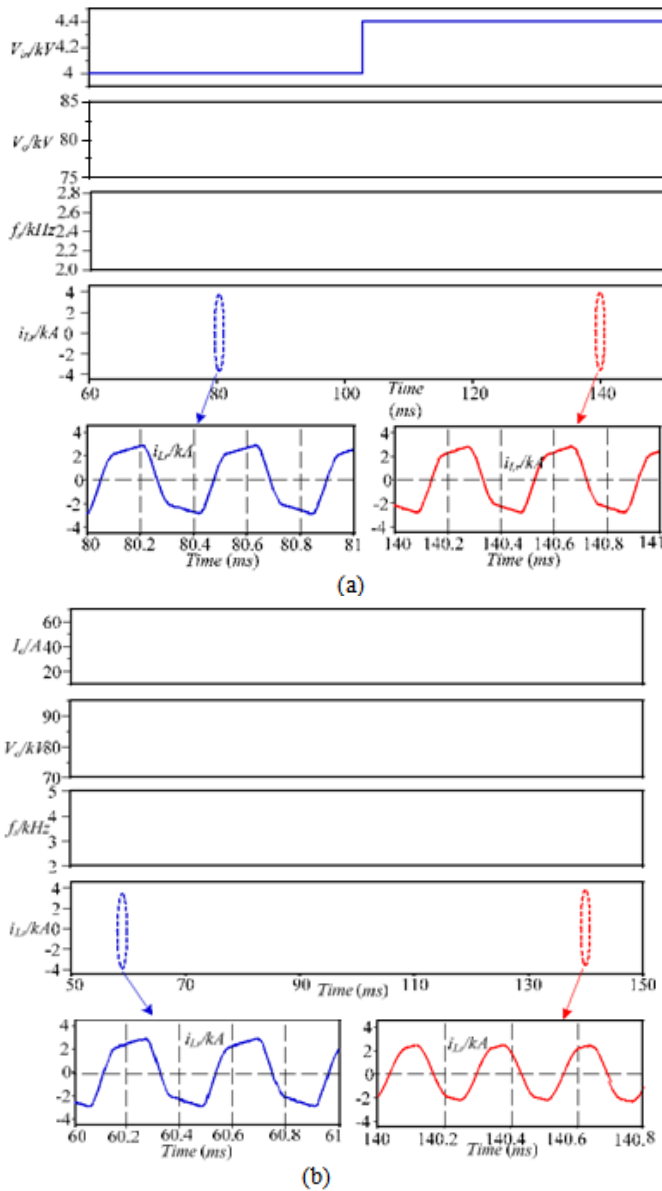


Figure 11. Dynamic simulation results. (a) Input voltage step. (b) Load step.

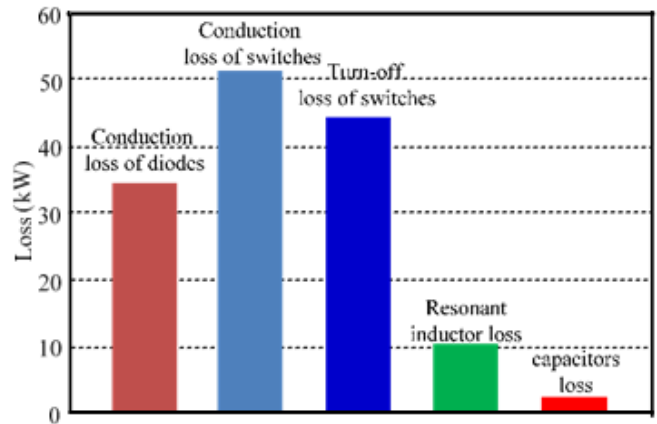


Figure 12. Calculated power losses distribution.

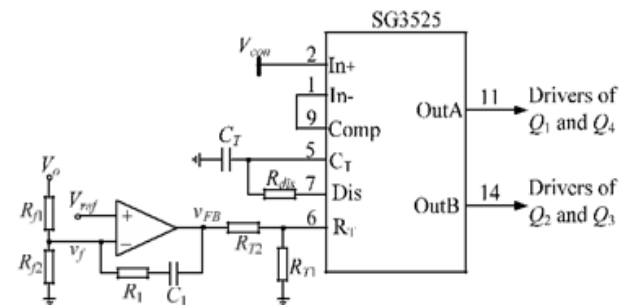
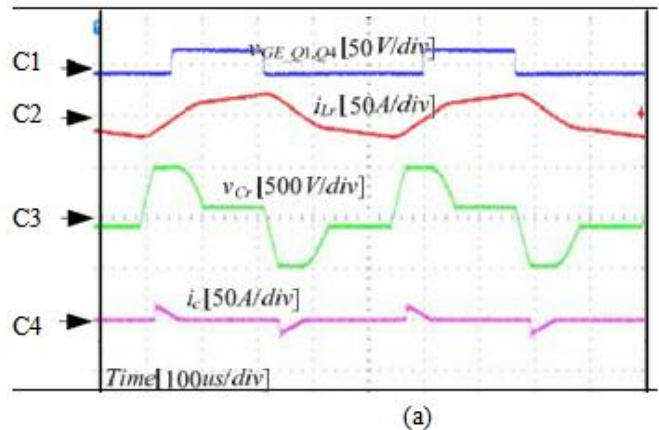


Figure 13. Block diagram of the control circuit.

It can be observed that the dominant part of the power losses is the conduction loss of diodes and switches. Although the turn-on loss is eliminated due to zero-voltage turn-on condition, because of the tail current characteristic, the turn-off loss of the IGBTs can only be alleviated thanks to the slow increasing of the voltage across the active switch. If the high-voltage large-current Silicon Carbide (SiC) MOSFET is available in the future [24], the turn-off loss the converter could be reduced significantly.



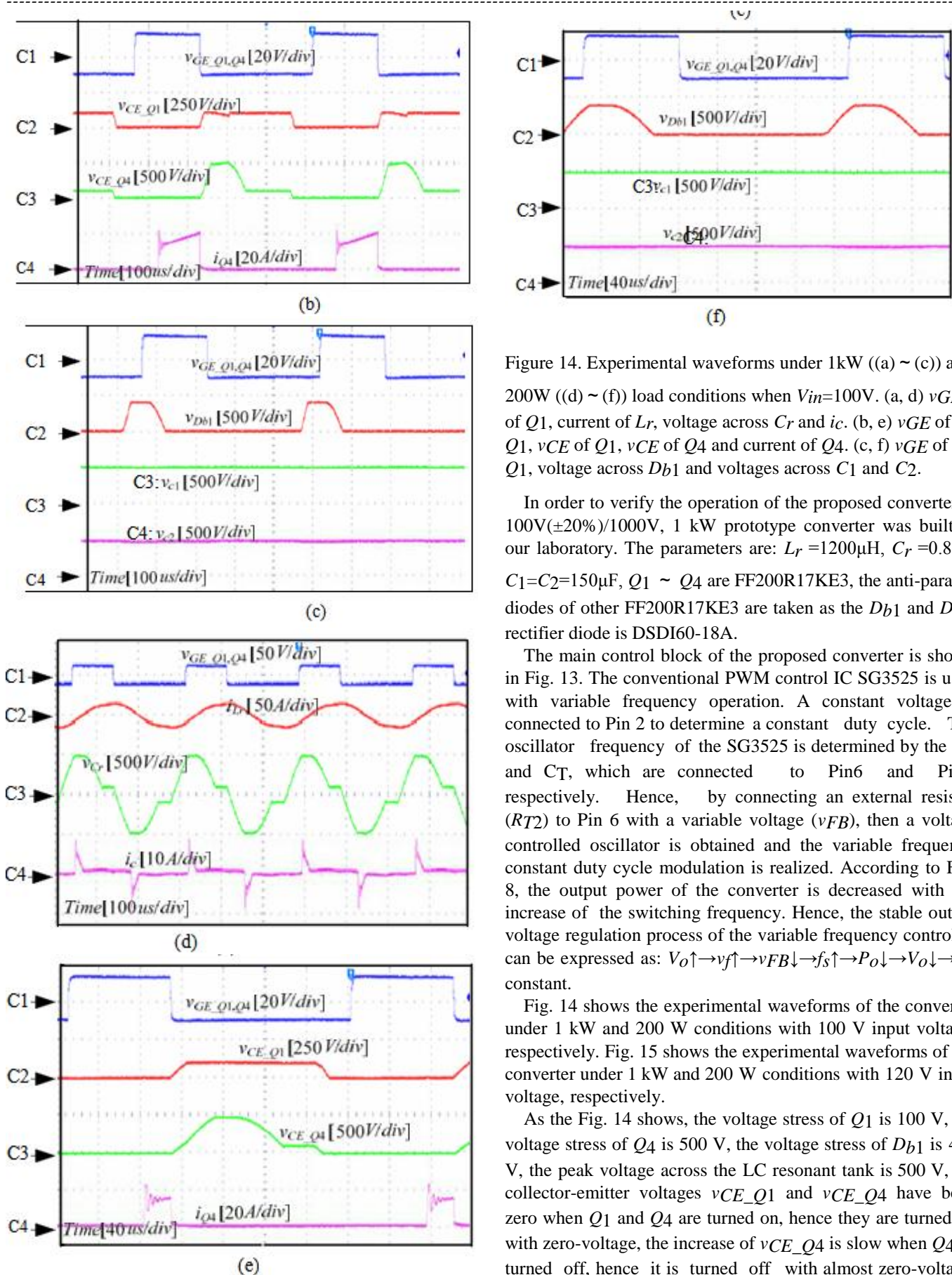


Figure 14. Experimental waveforms under 1kW ((a) ~ (c)) and 200W ((d) ~ (f)) load conditions when $V_{in}=100V$. (a, d) v_{GE} of $Q1$, current of L_r , voltage across C_r and i_c . (b, e) v_{GE} of $Q1$, v_{CE} of $Q1$, v_{CE} of $Q4$ and current of $Q4$. (c, f) v_{GE} of $Q1$, voltage across $Db1$ and voltages across $C1$ and $C2$.

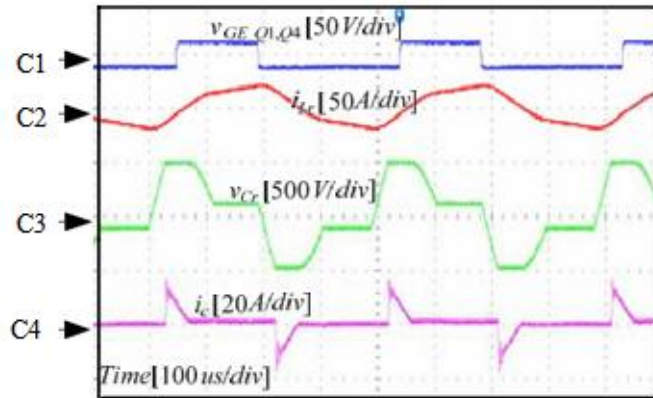
In order to verify the operation of the proposed converter, a 100V($\pm 20\%$)/1000V, 1 kW prototype converter was built in our laboratory. The parameters are: $L_r = 1200\mu H$, $C_r = 0.8\mu F$, $C_1 = C_2 = 150\mu F$, $Q_1 \sim Q_4$ are FF200R17KE3, the anti-parallel diodes of other FF200R17KE3 are taken as the $Db1$ and $Db2$, rectifier diode is DSDI60-18A.

The main control block of the proposed converter is shown in Fig. 13. The conventional PWM control IC SG3525 is used with variable frequency operation. A constant voltage is connected to Pin 2 to determine a constant duty cycle. The oscillator frequency of the SG3525 is determined by the R_T and C_T , which are connected to Pin6 and Pin5, respectively. Hence, by connecting an external resistor (R_{T2}) to Pin 6 with a variable voltage (v_{FB}), then a voltage controlled oscillator is obtained and the variable frequency constant duty cycle modulation is realized. According to Fig. 8, the output power of the converter is decreased with the increase of the switching frequency. Hence, the stable output voltage regulation process of the variable frequency controller can be expressed as: $V_o \uparrow \rightarrow v_f \uparrow \rightarrow v_{FB} \downarrow \rightarrow f_s \uparrow \rightarrow P_o \downarrow \rightarrow V_o \downarrow \rightarrow V_o$ constant.

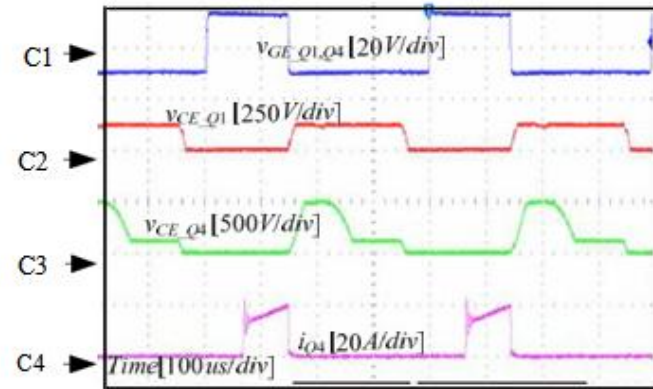
Fig. 14 shows the experimental waveforms of the converter under 1 kW and 200 W conditions with 100 V input voltage, respectively. Fig. 15 shows the experimental waveforms of the converter under 1 kW and 200 W conditions with 120 V input voltage, respectively.

As the Fig. 14 shows, the voltage stress of $Q1$ is 100 V, the voltage stress of $Q4$ is 500 V, the voltage stress of $Db1$ is 400 V, the peak voltage across the LC resonant tank is 500 V, the collector-emitter voltages $v_{CE_{Q1}}$ and $v_{CE_{Q4}}$ have been zero when $Q1$ and $Q4$ are turned on, hence they are turned on with zero-voltage, the increase of $v_{CE_{Q4}}$ is slow when $Q4$ is turned off, hence it is turned off with almost zero-voltage.

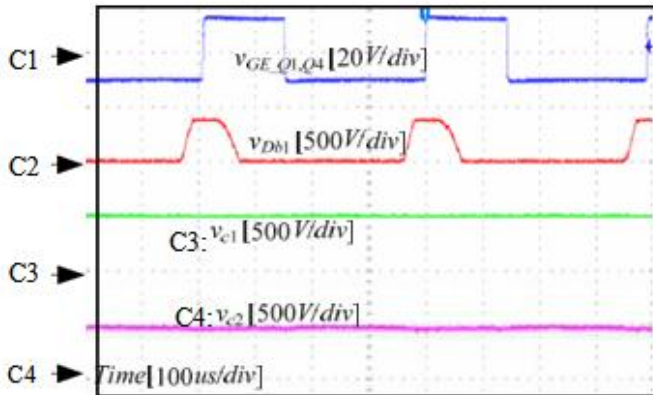
The oscillation of i_{Q4} is caused by the parasitic inductor of the prototype. All the waveforms agree well with the expected switching sequence in Fig. 2.



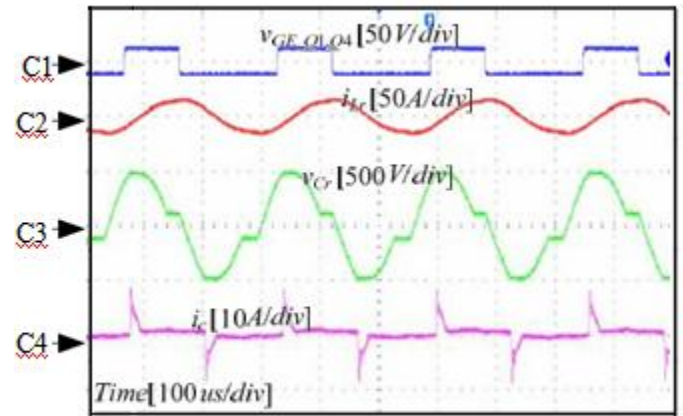
(a)



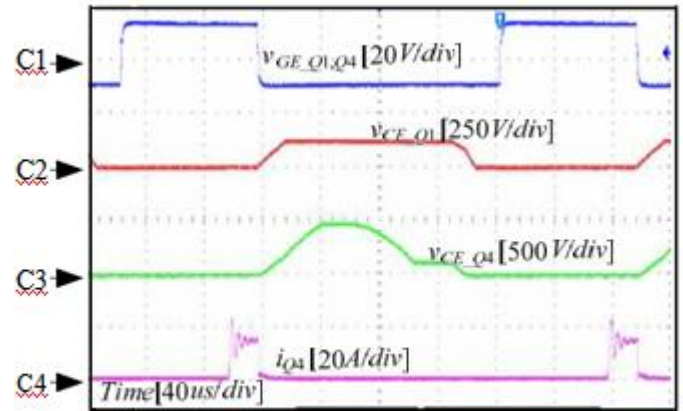
(b)



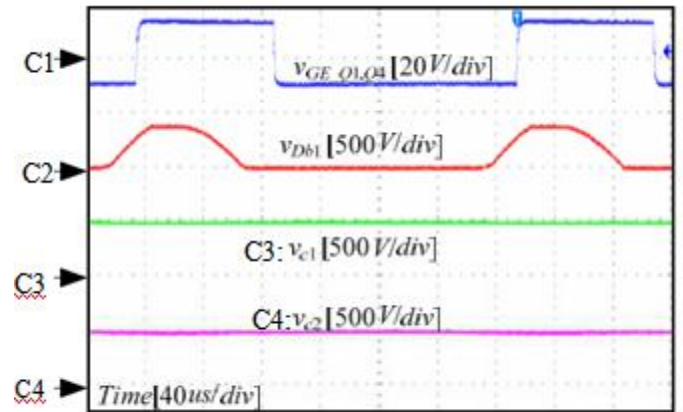
(c)



(d)



(e)



(f)

Fig. 15. Experimental waveforms under 1kW ((a) ~ (c)) and 200W ((d) ~ (f)) load conditions when $V_{in}=120V$. (a, d) v_{GE} of $Q1$, current of L_r , voltage across C_r and i_c . (b, e) v_{GE} of $Q1$, v_{CE} of $Q1$, v_{CE} of $Q4$ and current of $Q4$. (c, f) v_{GE} of $Q1$, voltage across $Db1$ and voltages across $C1$ and $C2$.

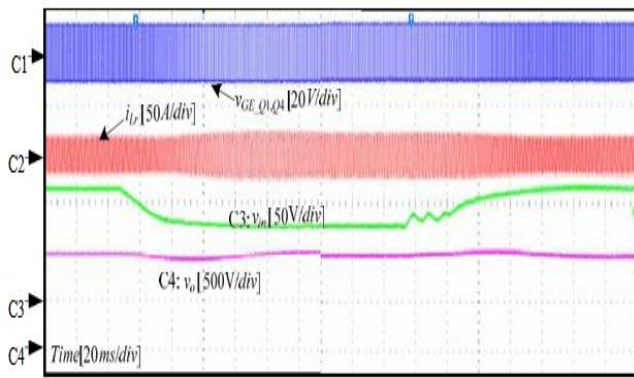


Figure 16. Experimental waveforms of an input voltage step change.

Fig. 16 illustrates the output voltage corresponding to a step change of input voltage varying between 80 V and 120 V.

Fig.17 illustrates the output voltage corresponding to a step change of load current varying between 1 A and 0.4 A. As seen, the output voltage can be regulated to be constant corresponding to the input voltage step change and load step change.

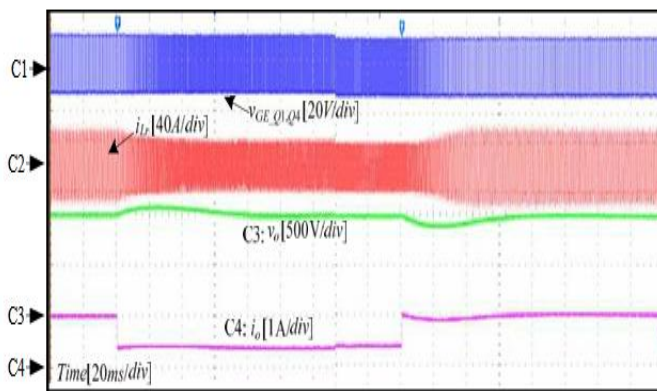
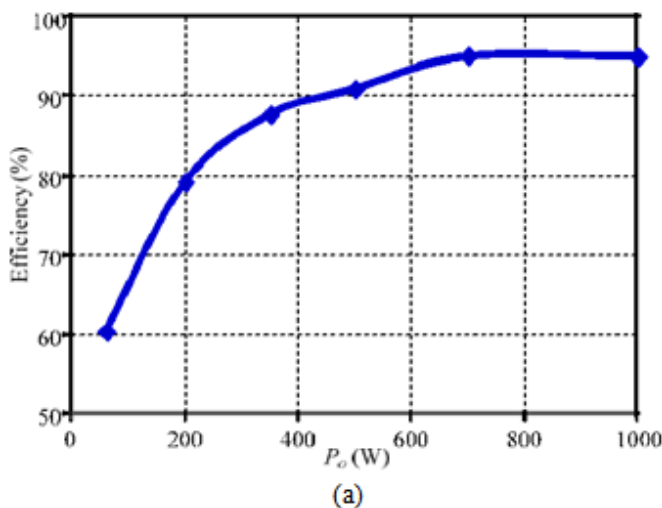
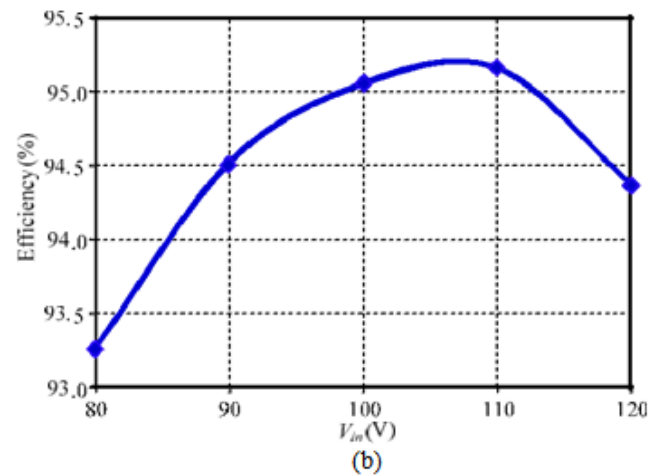


Figure 17. Experimental waveforms of a load step change.



(a)



(b)

Figure 18. Conversion efficiency of the proposed converter. (a) Efficiency at different output power under normal input voltage. (b) Efficiency at full load under different input voltages.

Figure. 18 shows the conversion efficiency of the proposed converter. Fig. 18(a) shows the efficiency at different output currents under normal input voltage of 100 V. Fig. 18(b) shows the efficiency at full load under different input voltages. It is shown that the maximum efficiency can be up to 95.2%.

As the Fig. 18(a) shows, the efficiency decreases with the decrease of the output power, because the switching frequency is higher at light load than that at heavy load (see Fig. 8), so the turn-off loss of switches increases at light load and is the main part of the loss.

For the constant output power, the average input current decreases with the increase of the input voltage, hence, the conduction loss will decrease with the increase of the input voltage. However, the switching frequency increases with the increase of the input voltage (see Fig. 8), hence, the switching loss (turn-off loss) will increase with the increase of the input voltage. So there is an optimum efficiency working point in the input voltage range, as shown in Fig. 18(b).

V. CONCLUSION

A novel resonant DC-DC converter is proposed in my work, which can achieves very high step-up voltage gain and it is suitable for high-power high-voltage applications. The converter utilizes the resonant inductor to delivery power by charging from the input and discharging to the output. The resonant capacitor is employed to achieve zero-voltage turn-on and turn-off for the active switches and ZCS for the rectifier diodes. The analysis demonstrates that the converter can operate at any gain value (>2) with proper control, however, the parameters of the resonant tank determine the maximum switching frequency, the range of switching frequency and current ratings of active switches and diodes. The converter is controlled by the variable switching frequency. Simulation and experimental results verify the operation principle of the converter and parameters selection of the resonant tank.

REFERENCES

- [1] CIGRE B4-52 Working Group, “HVDC grid feasibility study,” Melbourne: International Council on Large Electric Systems, 2011.
- [2] A. S. Abdel-Khalik, A. M. Massoud, A. A. Elserougi, and S. Ahmed, “Optimum power transmission-based droop control design for multi-terminal HVDC of offshore wind farms,” *IEEE Trans. Power Syst.*, vol. 28, no. 3, pp. 3401–3409, 2013.
- [3] F. Deng and Z. Chen, “Design of protective inductors for HVDC transmission line within DC grid offshore wind farms,” *IEEE Trans. Power Del.*, vol. 28, no. 1, pp. 75–83, 2013.
- [4] F. Deng and Zhe Chen, “Operation and control of a DC- grid off shore wind farm under DC transmission system faults,” *IEEE Trans. Power Del.*, vol. 28, no. 1, pp. 1356– 1363, 2013.
- [5] C. Meyer, “Key components for future offshore DC grids,” PhD Thesis, RWTH Aachen University, 2007.
- [6] W. Chen, A. Huang, S. Lukic, et al, “A comparison of medium voltage high power DC/DC converters with high step-up conversion ratio for offshore wind energy systems,” in *Proc. IEEE ECCE*, 2011, pp. 584–589.